December 1999 • NREL/SR-520-27664

Subcontractor Report

Nanostructure of a-Si:H and Related Alloys by Small-Angle Scattering of Neutrons and X-Rays

Annual Technical Progress Report
May 22, 1998 — May 21, 1999

D.L. Williamson
Department of Physics
Colorado School of Mines
Golden, Colorado

National Renewable Energy Laboratory

1617 Cole Boulevard
Golden, Colorado 80401-3393

NREL is a U.S. Department of Energy Laboratory
Operated by Midwest Research Institute • Battelle • Bechtel

Contract No. DE-AC36-99-GO10337

December 1999 • NREL/SR-520-27664

Nanostructure of a-Si:H and Related Alloys by Small-Angle Scattering of Neutrons and X-Rays

Annual Technical Progress Report
May 22, 1998 — May 21, 1999

D.L. Williamson
Department of Physics
Colorado School of Mines
Golden, Colorado

NREL Technical Monitor: B. von Roedern

Prepared under Subcontract No. XAK-8-17619-31

National Renewable Energy Laboratory

1617 Cole Boulevard
Golden, Colorado 80401-3393

NREL is a U.S. Department of Energy Laboratory
Operated by Midwest Research Institute • Battelle • Bechtel

Contract No. DE-AC36-99-GO10337

NOTICE

Available electronically at http://www.doe.gov/bridge

Available for a processing fee to U.S. Department of Energy
and its contractors, in paper, from:

U.S. Department of Energy
Office of Scientific and Technical Information
P.O. Box 62
Oak Ridge, TN 37831-0062
phone: 865.576.8401
fax: 865.576.5728
email: reports@adonis.osti.gov

Available for sale to the public, in paper, from:

U.S. Department of Commerce
National Technical Information Service
5285 Port Royal Road
Springfield, VA 22161
phone: 800.553.6847
fax: 703.605.6900
email: orders@ntis.fedworld.gov
online ordering: http://www.ntis.gov/ordering.htm

Printed on paper containing at least 50% wastepaper, including 20% postconsumer waste

1. EXECUTIVE SUMMARY

1.1 PREFACE

This report presents results of Phase I research performed from May 22, 1998 to May 21, 1999 under a cost-reimbursable subcontract from the National Renewable Energy Laboratory (NREL, a national laboratory of the U.S. Department of Energy operated by Midwest Research Institute) to the Colorado School of Mines (subcontract number XAK-8-17619-31 to the prime contract DE-AC36-83CH10093). The research was carried out under the direction of Don L. Williamson, Professor of Physics. Materials characterization, including small-angle x-ray scattering and x-ray diffraction were carried out in the Physics Department of the Colorado School of Mines. The materials for analyses were supplied by NREL-supported device-making groups as well as by other groups with relevant expertise. Electron microprobe analyses of film compositions were carried out by Alice Mason of NREL. The co-P.I., David Marr, of the Chemical Engineering Department of the Colorado School of Mines, contributed to the research project via assistance in the preparation of the proposal to NIST for the small-angle neutron scattering experiments and via assistance in the design of the samples for these experiments.

1.2 OBJECTIVES/APPROACH

The general objective of this research is to provide detailed microstructural information on the amorphous-silicon-based, thin-film materials under development for improved multijunction solar cells. Correlation of this microstructure with opto-electronic properties and device performance is an integral part of the research. The principal experimental techniques used are small-angle x-ray scattering (SAXS), small-angle neutron scattering (SANS), and conventional x-ray diffraction (XRD). These provide quantitative microstructural data on microvoid fractions, sizes, shapes, preferred orientations, hydrogen clustering, microcrystallinity, and medium-range order. An important task is to establish whether SANS can be used to determine the hydrogen nanostructure and any changes that might occur due to light soaking. Some experiments are conducted using anomalous SAXS (ASAXS) via special facilities in Germany. This method provides information on the Ge uniformity and nanostructure in a-SiGe:H alloys. Two types of material have been investigated during this first phase of the research in collaboration with the NREL Low-gap and Mid-gap/Metastability National Teams.

1.3 CONCLUSIONS and STATUS of SANS EXPERIMENTS

1.3.1 Mid-Gap Materials

Medium-range order - Analysis of the first (lowest angle) scattering peak of the a-Si:H phase demonstrates that its width, directly related to medium-range order (MRO), is reduced by heavier hydrogen dilution in PECVD growth or by increased substrate temperature in HWCVD growth. The narrowest width (and therefore best MRO) of fully amorphous material correlates with better solar cell stability and this is not likely related to bonded hydrogen content since it is quite different in the optimized PECVD and HWCVD a-Si:H. A wide range of MRO apparently exists in the residual amorphous phase of the mixed amorphous/microcrystalline material.

Microcrystallinity - High-hydrogen-diluted films of PECVD a-Si:H that are 0.5 μm in thickness and optimized for solar cell efficiency and stability, are found to be partially microcrystalline (μc) if deposited directly on stainless steel (SS) substrates but are fully amorphous if a thin n layer of a-Si:H or μc-Si:H is first deposited on the SS. In these latter cases, partial microcrystallinity develops as the films are grown thicker (1.5 - 2.5 μm) and this is accompanied by sharp drops in open circuit voltage.

SAXS from NREL HWCVD a-Si:H - A dramatic increase in nanovoid volume fraction was observed in HWCVD films when the substrate temperature was lowered from 360 to 280°C.

SAXS from MVS PECVD and HWCVD a-Si:H - A large difference is seen in the nanostructure of PECVD and HWCVD films prepared by MVSystems. The HWCVD sample is dominated by larger scale (>10 nm) structure while the PECVD sample shows only small scale structure (~1 nm). Both have low void contents near 0.1 vol.%.

Effect of Deposition Rate on Nanostructure via RF- and VHF-PECVD of a-Si:H - A comparison of the nanostructure from 13.56 MHz-deposited films and 70 MHz-deposited films shows that the VHF 70 MHz technique produces more homogeneous films at higher deposition rates. For example, a 70 MHz film deposited at 1 nm/s has only half the void fraction as a 13.56 MHz film deposited at 0.6 nm/s.

1.3.2 Low-Gap Materials

Thickness dependence of nanostructure in a-SiGe:H - Based on studies of a set of three samples from ECD, one prepared with a special multilayer structure, there is no detectable difference in the nanostructure between 0.2-μm- and 1.3-μm-thick films.

1.3.3 Status of SANS Experiments

Proposal for Beam Time - In response to a request for beam time proposals from the NIST Center for Neutron Research, a proposal for SANS was prepared and submitted by the March 1, 1999 deadline. The proposal was peer-reviewed and awarded beam time of 3 days in August, 1999.

Sample Preparation - A carefully designed set of samples is being prepared by NREL (HWCVD) and by USSC (PECVD) for the SANS experiments. Deuterated gases (SiD_4, GeD_4 and D_2) have been supplied to the film growers. Special c-Si substrates with surface roughness less than 0.5 nm rms will be used. Preliminary experiments have been made to establish the substrate pre-treatment conditions and the maximum thicknesses that can be deposited without delamination. Some of the films will be put in the light-soaked state prior to the SANS experiments so that SANS measurements followed by in-situ annealing and further SANS can be performed to look for any light-induced structural change.

Table of Contents

List of Figures

List of Tables

2. INTRODUCTION

Several experiments have been completed during Phase I of this research project in collaboration with NREL and NREL-supported groups. The planned SANS studies have been delayed due to an unexpected shut-down of the research nuclear reactor at the NIST Center for Neutron Research in Gaithersburg, Maryland. However, the facility is again operational and SANS beam time has been awarded to us for three days beginning on August 9, 1999. A summary of the samples being prepared for this experiment will be presented below. The results and discussion of the in-house SAXS and XRD experiments will be broken into sections according to whether the materials are low-gap, mid-gap, and high-gap, consistent with the NREL team structure. We have not received any high-gap materials for study during Phase I.

Several experiments were done with mid-gap materials. A systematic study of the medium-range order (MRO) of PECVD and HWCVD a-Si:H films was done in collaboration with USSC, University of Oregon, and NREL. Discoveries were made on microcrystalline (μc)-Si:H formation in highly-hydrogen-diluted material prepared by USSC, depending on substrate and film thickness. The HWCVD material being prepared in the tube (T) system at NREL was investigated by SAXS. New material being grown by MVSystems using both PECVD and HWCVD (via a special hot filament) has been examined by SAXS. Recently, a systematic study was begun in collaboration with ECD to compare the nanostructures of RF and VHF a-Si:H deposited at increased deposition rates. Some initial results from this SAXS study are presented below. In the area of low-gap materials, an experiment was carried out in collaboration with ECD to determine whether there is any thickness dependence in the SAXS-detected nanostructure of a-SiGe:H low-gap films.

3. RESULTS AND DISCUSSION

3.1 MID-GAP MATERIALS

3.1.1 Medium-range order in a-Si:H below and above the onset of microcrystallinity

Introduction- There is a growing body of experimental evidence that the best device-quality a-Si:H materials have some type of improved, or at least modified, structural order as determined or inferred by a variety of techniques [1-21]. All of these studies can be divided into two deposition methods being used to reach these new levels of order: (i) high hydrogen dilution of silane or disilane in the plasma-enhanced chemical vapor deposition (PECVD) method [1-12] or (ii) elevated substrate temperatures in the hot-wire chemical vapor deposition (HWCVD) method

[13-21]. These two types of films are dramatically different in hydrogen content, ranging from 7 to 16 at.% for the PECVD H_2-diluted films and from less than 1 at.% to about 4 at.% for the HWCVD high-substrate-temperature films. It is also interesting that the deposition rates of the HWCVD process (~1 nm/s) are significantly faster than those from the PECVD process (≤0.3 nm/s), for fabrication of films of comparable opto-electronic quality. In the above studies, structural characteristics have been inferred from NMR (hydrogen distributions), Raman (short-range order), IR (hydrogen bonding configurations), spectroscopic ellipsometry (film nucleation, growth, and microcrystallinity), AFM (surface topography), internal friction, Urbach energy, hydrogen evolution, residual stress, and mass density. Several of the studies have used the more direct structural methods of transmission electron microscopy (TEM) [4,5,10,11,21] and x-ray diffraction (XRD) [7,10,12,18]. High-resolution TEM has provided direct evidence of ordered regions on the nanometer scale within the amorphous matrix of the high-hydrogen-diluted PECVD material [4,5,10] and cross-sectional TEM of HWCVD material shows the onset of crystallinity near the substrate with increasing film thickness [21]. In addition to providing direct information on the degree of microcrystallinity [7,10,12] and its sensitivity to the nature of the substrate [12], XRD has recently been used to show direct evidence of improved medium-range order in both the elevated-substrate-temperature HWCVD material [18] and in the high-hydrogen-dilution PECVD films [12]. This approach involves a careful examination of the width of the lowest angle x-ray scattering peak from the a-Si:H matrix. Here we will provide more details and results of such studies, with a more complete comparison of data from the PECVD and HWCVD materials, after first providing a brief review of the concept of medium-range order, particularly as detected by XRD.

Medium-range order - Medium-range order (MRO) is a term used to discuss the structural ordering of amorphous systems on a length scale larger than nearest neighbor distances (short-range order) up to an ill-defined upper limit around 2 to 5 nm. MRO has received a great deal of attention recently with respect to amorphous covalent glasses. Most of the focus has been on the oxide and chalcogenide glasses due to the "pre-peak" or "first sharp diffraction peak (FSDP)" or "first scattering peak (FSP)" in the x-ray and neutron diffraction patterns as described in review articles [22-25] that reveal the considerable controversy on this topic. This feature occurs at unusually low scattering angles or momentum transfer, $q \approx 10$ to 20 nm^{-1}, $q = (4\pi\sin\theta)/\lambda$, where 2θ is the scattering angle and λ is the radiation wavelength. There has been some modeling research

[26-28] directed specifically to understanding the FSP of a-Si and a-Si:H which occurs near the upper end of the q-range associated with MRO (q=19.5 nm^{-1}, or at $2\theta \approx 27.6°$ when λ=0.154 nm, i.e. Cu-K_α x-rays). It is interesting to note that this peak has little to do with the (111) Bragg diffraction peak of c-Si despite its similar location at q = 20.0 nm^{-1} [28] or with diffraction associated with the well-defined nearest neighbor distance in a-Si since, via the Bragg law, this nearest neighbor distance would produce a scattering peak at $q \approx 2\pi/0.235$ nm = 26.7 nm^{-1}. The latter q is actually near the *minimum* between the first and second scattering peaks of a-Si (and a-Si:H) [26-28].

Calculations based on various a-Si structural models [26-28] clearly demonstrate that the FSP has significant contributions from MRO, while the higher q peaks have little sensitivity. Most recently, Uhlherr and Elliott [28] have shown that weak oscillations in the real-space pair distribution function g(r) of a-Si extending from r = 1.0 to 3.3 nm contribute about half the intensity of the FSP. The partial pair distribution functions based on next-nearest neighbor separation seems to play the dominant role leading to this extended range order [28]. These studies make it clear that an experimental focus on the FSP of a-Si:H should lead to information on the MRO and, indeed, this was recognized several years ago [29] and applied to comparisons of a-Si:H prepared by sputter-deposition and PECVD. A simple, experimental, quantitative measure of the correlation length, L, over which the atomic density fluctuations contribute to this FSP can be obtained from its width, W (full-width-at-half-maximum intensity in radians), via the Scherrer equation [30], $L= 0.9\lambda/W\cos\theta$, or via a nearly equivalent expression [25,31], $L = 2\pi/\Delta q$, where Δq is the width of the peak in nm^{-1}. The Scherrer equation is most often used to estimate the average crystallite size of microcrystalline (μc) Si.

Another x-ray scattering technique used to provide detailed structural information on a-Si:H and related thin-film materials is small-angle x-ray scattering (SAXS) occurring at very low q [32]. However, this information is more appropriately characterized as medium- or extended-range *disorder*, associated with inhomogeneities in the films such as nanovoids and columnar-like growth features [32]. Studies of both the high-hydrogen-diluted PECVD and elevated-temperature HWCVD materials of interest here demonstrated undetectable levels of inhomogeneities on the nanoscale (void volume fractions less than 0.01%), but evidence of larger-scale features (> 20 nm), probably associated with residual columnar-like structure or surface roughness [2,32].

Recently, a new TEM method has been developed to examine MRO in amorphous materials [33] and evidence has been found for changes in MRO in a-Si:H induced by light soaking [34].

Experimental methods - Numerous PECVD and HWCVD a-Si:H films have been prepared for XRD on stainless steel (SS) substrates, both because of the weak interference of the SS with the FSP in the XRD data and because this is a common substrate for the best solar cells made from these materials [2,35,36]. Several series of PECVD undoped (intrinsic - i) films were made to explore effects of hydrogen dilution (none, low, high), film thickness (0.5 μm to 2.5 μm), and substrate nature (bare stainless steel - i/SS, amorphous n-layer-coated stainless steel - i/μ-n/SS, and microcrystalline n-layer-coated stainless steel - i/mc-n/SS). The n-layers were typically about 20 nm thick. For XRD the films were deposited on 2.5 cm x 2.5 cm stainless steel (SS) substrates providing adequate area for good diffraction signals. The level of hydrogen dilution in the "high-hydrogen-dilution" i-layers studied here are similar to those used in recent world-record-efficiency solar cells [35]. Some of the films have been further processed to examine solar-cell open circuit voltages, V_{oc}, and defect concentrations via drive-level capacitance profiling and these results have been recently presented in correlation with XRD results [12]. Three series of HWCVD films have been prepared [13] in two different deposition systems and with different filament currents, typically to a thickness of 1-2 μm. All three series were made with substrate temperature as the deposition variable. XRD and Raman experiments with one series have been reported earlier [18].

The XRD measurements were carried out in the symmetric Bragg-Brentano geometry operating with Cu-K_α radiation as selected by a graphite monochromator in the scattered beam. The instrumental linewidth in the region of the FSP of a-Si:H is $W_i = 0.12°$ based on measurements using a NIST LaB_6 reference powder. The width used in the Scherrer equation (given above) is typically $W = (W_m^2 - W_i^2)^{1/2}$, where W_m is the measured width from the sample. Since the absorption length of this 0.154 nm radiation is about 70 μm in Si, most of the scattering signal originates from the SS substrate. However, this signal is strongly localized in the bcc/fcc diffraction peaks and some secondary phase peaks, none of which interfere with the FSP (located near $2\theta = 27.6°$) from a-Si:H nor with the (111), (220), or (311) c-Si diffraction peaks. Long counting times were used to achieve good signal-to-noise and the bare SS substrate signal was subtracted from each XRD pattern (with appropriate absorption corrections). Since the SS apparently has different degrees of polycrystalline texture for the various samples, this would not typically remove the

strongest bcc peaks at 2θ = 44° and 65°. These were then removed by a smoothing procedure in order to examine more carefully the a-Si:H and μc-Si:H peaks. The full-width-at-half-maximum intensity (W_m) of the FSP of a-Si:H, as well as the fractional area (integrated intensity) of the μc-Si:H (111)+(220)+(311) peaks compared to that of the total area from 15° to 65° were extracted via a least-square fitting routine based on a superposition of Voigt line-shape functions. This function is symmetric but has two width parameters used to adjust the shape. Typically the second a-Si:H peak centered near 2θ = 51° was included in the fit due to the slight overlap of its low-angle tail with the FSP. To account for some slight asymmetry in this second peak, a third peak was included at a fixed angle near 45° in all fits of fully amorphous films. An example of the data and this type of fit is shown in Fig. 1 for a fully amorphous film. Also shown is a fit to a partially microcrystalline film where the sharper (111), (220), and (311) peaks of the μc phase are indicated. The residual amorphous phase FSP remains clear enough to track its width in the partially microcrystalline material.

Results and discussion

PECVD Material

Figure 2 demonstrates the substrate sensitivity of the high-H_2-diluted PECVD films to the formation of partially μc material. These films were all made under nominally identical conditions and grown to a common thickness of 0.5 μm. One can see that the presence of the thin intermediate a-n or μc-n layer on the SS prevents the partial microcrystallinity, at least to the sensitivity level of the XRD which is estimated to be about 2 to 4 vol.% for the data shown. The latter estimate is based on the result that the fractional areas of the mc peaks for the two samples shown are 10% and 15% so that 2 to 4% should still be detectable within the counting statistics obtained. Duplicate runs are shown to demonstrate reproducibility of the effect. Sensitivity of microcrystallite formation to the type and morphology of the substrate has been demonstrated by others [9,37-41]. Somewhat similar to the present result, deposition on a pre-deposited a-Si:H layer apparently hinders microcrystallinity [9,37,40], although increase in dilution [9], longer hydrogen plasma treatment [37], or higher plasma frequency [40] leads to initiation of microcrystallinity even on this self-similar substrate.

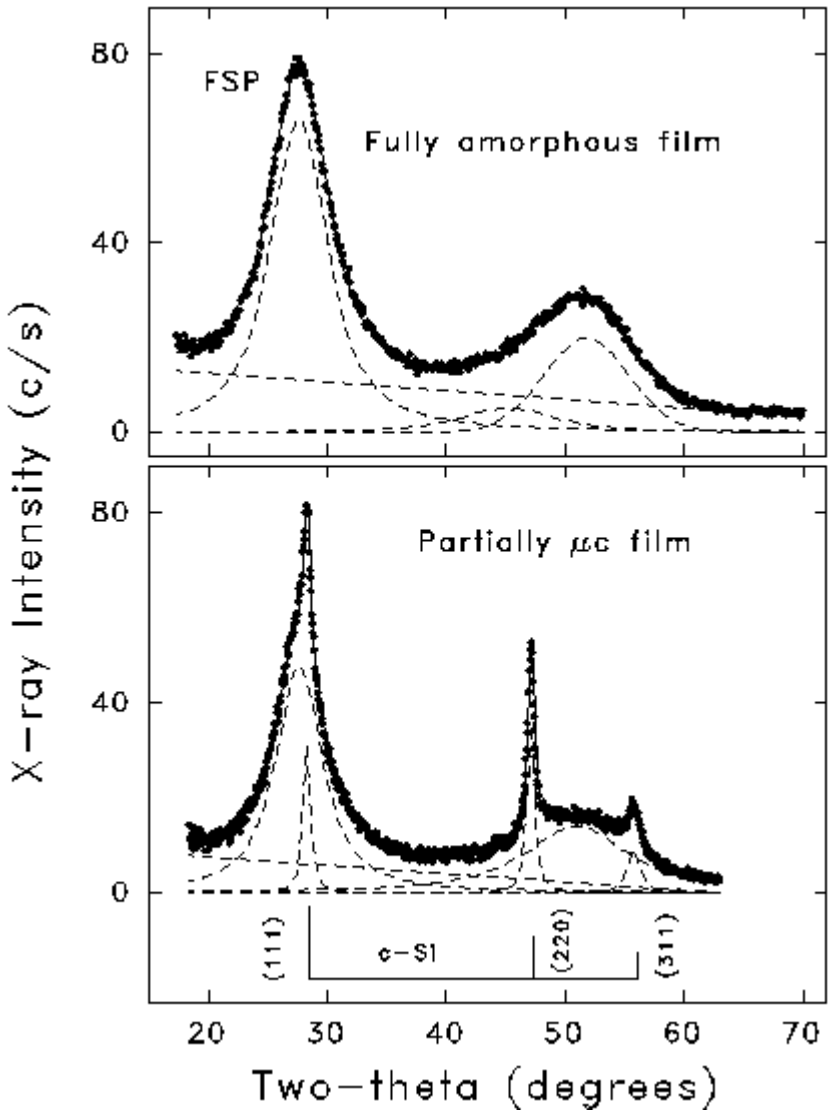

FIG. 1. Example least-square fits of X-ray diffraction patterns from the two type of films studied here, completely amorphous-Si:H (with the first scattering peak, FSP, indicated) and mixed amorphous/microcrystalline. Superpositions of Voigt line-shape functions and a linear background were used as indicated by the dashed curves to generate the solid line fit through the data. The stick diagram for randomly-oriented c-Si is shown with the lowest 3 Bragg peaks.

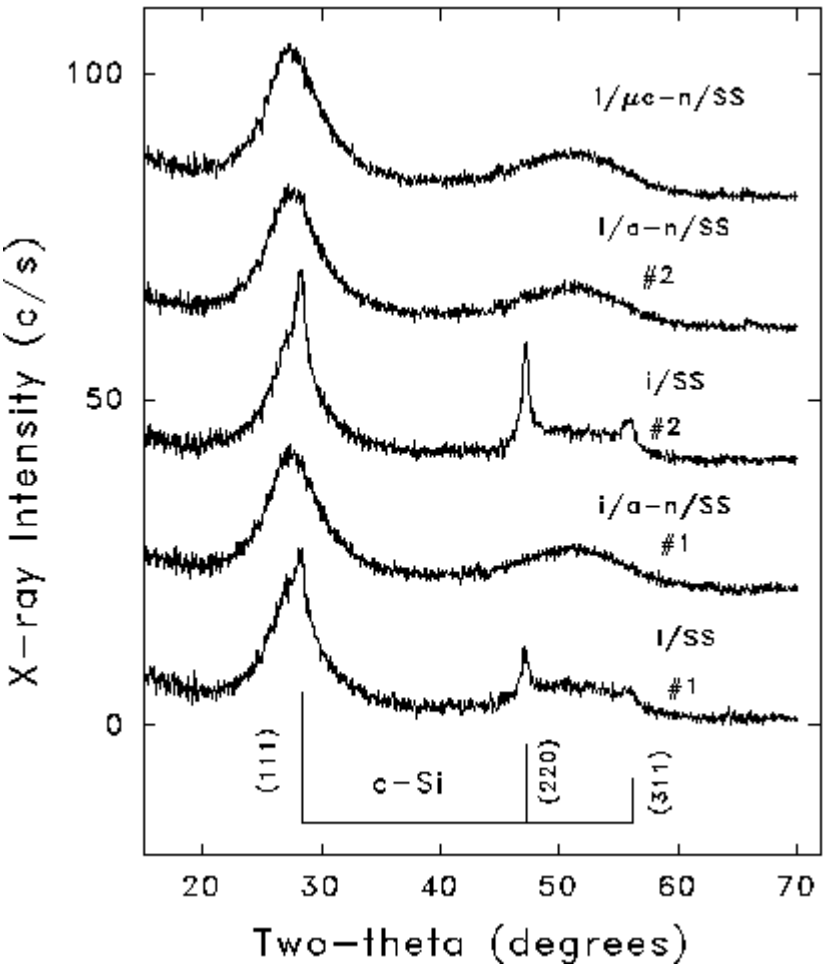

FIG. 2. X-ray diffraction patterns from a series of i-layers on SS, and μc-n coated SS, and μc-n coated SS. All i-layers were grown under identical high-hydrogen-dilution PECVD conditions and all are 0.5 μm thick. Duplicate runs are indicated.

A series of films made with increasing thickness under nominally identical high-hydrogen-dilution conditions on the a-n coated SS shows a transition to partially μc material as demonstrated in Fig. 3. Also shown is a thick film made at low dilution that remains fully amorphous. Thus, between 0.5 and 1.5 μm the intrinsic a-Si:H becomes partially microcystalline under the high dilution condition. From the widths of the μc peaks, the grain sizes via the Scherrer formula given in the experimental section are 6 to 22 nm, depending on orientation. The thicker 2.5 μm film develops a strong preferred orientation of the (220) planes parallel to the film surface as indicated by its much stronger relative intensity compared to the random c-Si intensities shown by the stick diagram in Fig. 2. These grains also tend to be at the large end of the size range. The transition to partially μc-Si:H is accompanied by large drops in the open circuit voltage, V_{oc}, for devices made by completion of a p-i-n structure on co-deposited films [12]. In addition, defect levels as determined by capacitance measurements [12], tend to decrease with distance from the substrate, suggesting improved order with thickness. Supporting the transition thickness shown in Fig. 3, photocapacitance spectra show the onset of microcrystallinity between 1.0 and 1.3 mm for films made under the same high-dilution conditions used for the XRD studies [12].

Although others have examined thickness effects on the structure of a/μc-Si:H [6,9, 21,39,40], the work by Koh et al [6,9] is particularly relevant to the present results since hydrogen dilution levels and substrate effects were examined in connection with the onset of microcrystallinity versus film thickness. A thickness versus hydrogen dilution "phase diagram" was proposed [9] in which a phase boundary exists between amorphous and microcrystalline material. For their deposition system, this phase boundary was explored via spectroscopic ellipsometry below about 200 nm down to 10 nm for H_2/SiH_4 gas ratios up to 80. This phase diagram led to the development of a two-step process for solar cell fabrication whereby an initial growth of the i-layer was done at high dilution to begin this layer close to but below the onset of μc-Si:H formation, followed by a reduction of the dilution ratio to finish the layer to remain in the fully amorphous state, but again close to the onset. The region of the phase diagram near the phase boundary, but below the onset, was termed the "proto-crystalline" regime [9]. Improved device behavior was demonstrated with this two-step procedure [9]. Although the present results are far from the phase boundary in the 10 nm thickness regime, it is clear that such a boundary exists between 0.5 and 1.3 μm for the high-dilution condition on the a-n/SS substrate and it is shifted to less than 0.5 μm on the bare SS.

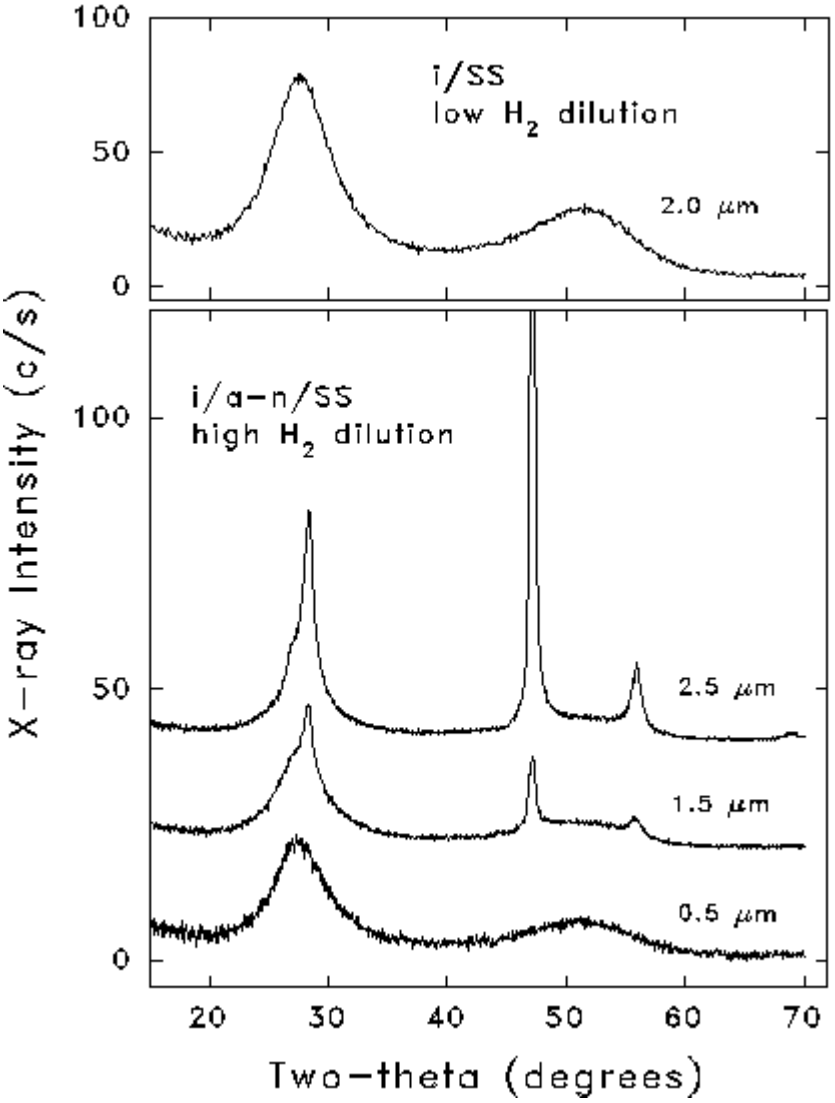

FIG. 3. X-ray diffraction patterns from series of i-layers grown under identical high-hydrogen-dilution PECVD conditions on a-n coated SS grown with increasing thickness as indicated. The top pattern shows no evidence for microcrystallinity under the low-hydrogen-dilution condition. The intensities of the 1.5 and 2.5 μm films have been divided by 3 and 5, respectively, for better comparison to the 0.5 μm film.

Evidence for improved structural order is presented in Fig. 4 in exactly the same regime suggested as "proto-crystalline" in nature [9]. The width of the FSP is displayed as a function of the amount of microcrystalline material in each PECVD sample as determined by the fractional area of the (111)+(220)+(311) diffraction peaks. Note that there are several samples shown that are fully amorphous but they fall into two groups, a broader-width band above 5.5° associated with the low- and no-hydrogen-diluted material and a narrower-width band between 5.0° and 5.4° generated by the high-hydrogen-diluted films. All films with some μc fraction then fall below a rather well-defined "onset width" value of W = 4.95 ± 0.1° as indicated by the dashed line in Fig. 4. The width of the FSP decreases systematically with increasing microcrystallinity. Using the Scherrer equation to estimate changes in correlation length associated with the MRO, the right hand scale shows that the correlation length increases by about a factor of two from 1.4 to 2.8 nm for the range of W's observed. The improvement in MRO associated with the fully amorphous material covers a rather modest range of just over 0.2 nm, or about a 15% change. However, this improvement seems to be correlated with improvement in device properties as will be discussed after the HWCVD data are included.

A comparison with earlier PECVD material is possible from the XRD study of Dixmier et al [27,29] which correlated the Urbach energy of a-Si:H prepared by both PECVD and sputtering with the width of the FSP. A plot was made based on the Scherrer equation and it was observed that the PECVD material was grouped at the longer correlation end of the trend, with Urbach energies approaching 50 meV. It is interesting that the longest length corresponds to W = 5.8° (for $\lambda = 0.154$ nm) which is in agreement with the present results in Fig. 4 for the low- or no-dilution materials. An Urbach energy for the present high-dilution PECVD material was measured to be 46 meV [12]. The sputtered material showed Urbach energies up to about 170 meV and shorter correlation lengths corresponding to W's up to 8.9°, much larger than the PECVD material.

A look at the position of the FSP is warranted based on earlier evidence of a sensitivity to network relaxation [27]. The peak remains located in the narrow range 27.6 ± 0.1° for all the fully amorphous films and the group of partially μc films with fractions below 20% (Fig. 4) but increases slightly to the range 27.9 ± 0.1 for the group with higher fractions (45 - 67%).

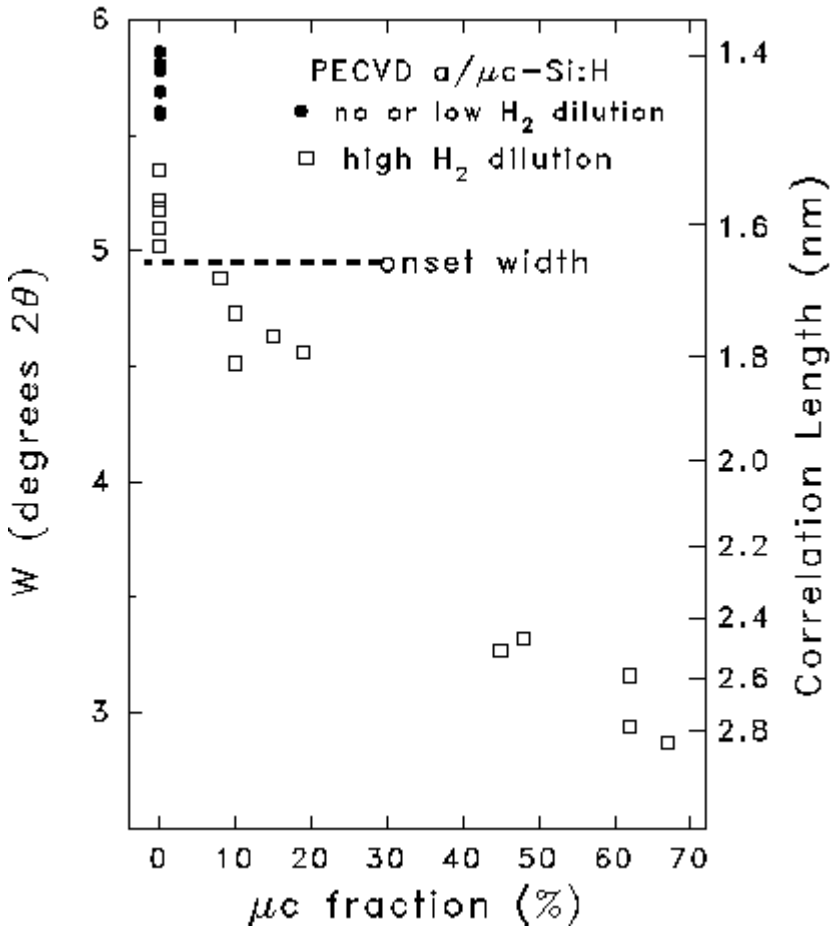

FIG. 4. Summary of XRD width values for the FSP of PECVD a-Si:H. Right-hand scale is based on Scherrer equation. The μc fraction is estimated from the fitted XRD integrated intensities of the (111)+(220)+(311) Bragg peaks as described in the experimental section.

HWCVD Material

Evidence of improved MRO in HWCVD a-Si:H was obtained by variation of the substrate temperature, T_s, during deposition [18]. The width of the FSP was shown to decrease systematically with increasing T_s. The same samples were studied by Raman spectroscopy and no evidence was found for improvements in the SRO based on the width of the Si-Si TO mode [18]. The XRD data are reproduced in Fig. 5 along with new data from HWCVD films made with a different system ("tube" system vs the earlier "cross" system). The solid curve guides the eye through the earlier data and dashed lines show the trends for two series of HWCVD films made with two different filament currents (14 and 16 A). There seems to be a slight difference in the trends for the two different HWCVD deposition systems, but both show improvements in MRO with increasing T_s. All the HWCVD material was made without any hydrogen dilution and all of the films remained fully amorphous. However, similar to the PECVD trend, using hydrogen dilution leads to microcrystalline material [42] and there is recent evidence for a thickness-induced transition to the partial mc state [21], however at a thickness of only about 70 nm for the conditions used.

A detailed comparison with the PECVD film results is now made by adding these data to Fig. 5 along the vertical line at T_s = 300°C where all these films were made. The V_{oc}'s obtained [12] are also shown for the three groups of PECVD samples (fully amorphous, low μc fraction, and high μc fraction - as indicated in Fig. 4). All the values for the fully amorphous films remain uniformly high (0.9 to 1.00 V). One can see that the low- and no-hydrogen-dilution widths are the same as the HWCVD film widths for a similar substrate temperature but the high-dilution widths clearly fall below the HWCVD trends. The reader is reminded that the higher-temperature HWCVD material is that which is of interest for device applications due to evidence of improved light stability [36,43]. Also, the high-hydrogen-dilution PECVD material is being used to produce the best and most stable solar cell efficiencies to date [2,35]. Figure 5 therefore suggests a band of FSP width (shaded region) that is associated with the best device material made by *either* PECVD or HWCVD methods. This band represents the best MRO possible, as determined by XRD, before the onset of microcrystallinity and the associated reductions in V_{oc} [12] as indicated in Fig. 5.

Summary - Focus on the first x-ray scattering peak of a-Si:H made by recent state-of-the-art methods has provided direct evidence of improved MRO in the materials presently being used as

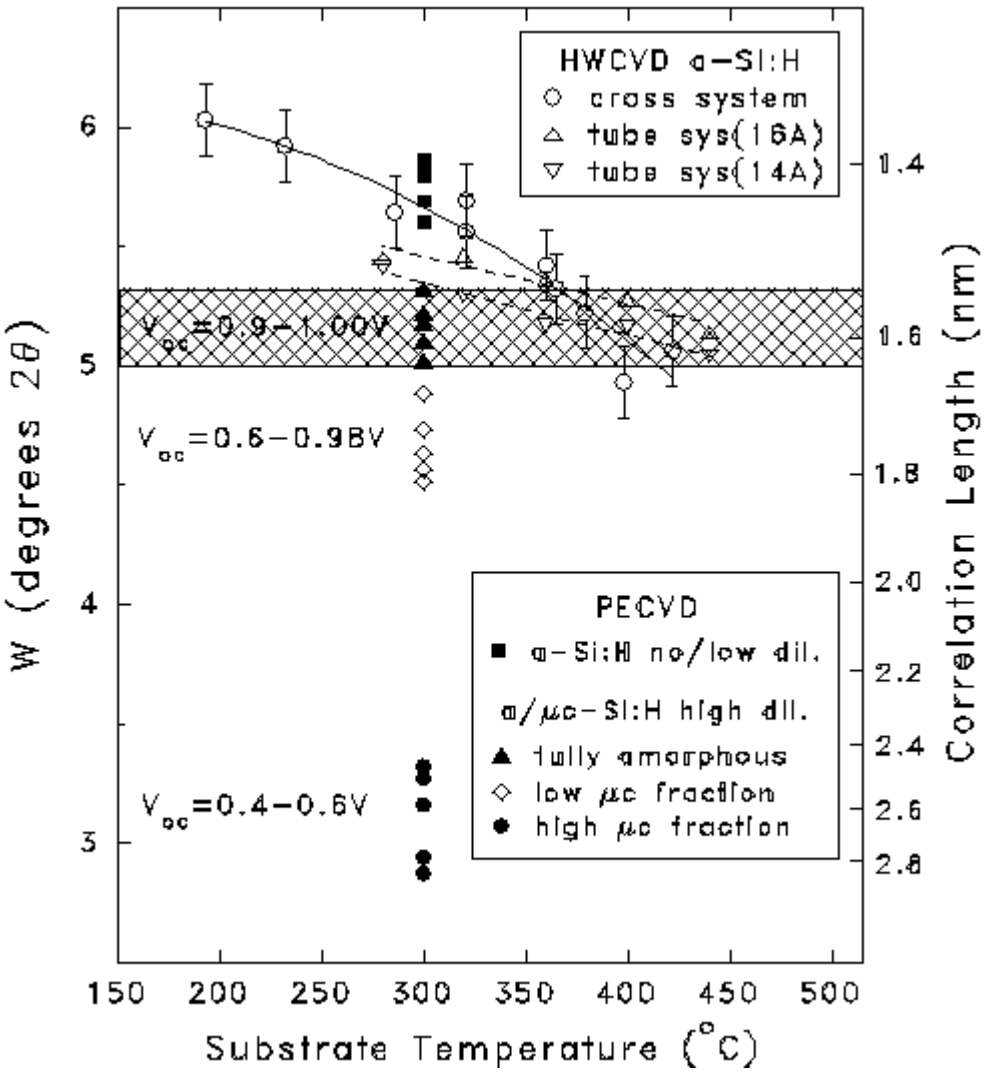

FIG. 5. Comparison of XRD FSP widths for HWCVD and PECVD i-layer films. The HWCVD films were made at various substrate temperatures while the PECVD films were all made at 300°C. The open circuit voltages shown were all obtained from co-deposited PECVD films (via completion of a p-i-n dot solar cells [12]).

i-layers in the best solar cells fabricated by each method. These improved materials lie just below the boundary of the transition to the microcrystalline state, consistent with the concept of a proto-crystalline regime [9]. Although PECVD and HWCVD deposition conditions have been developed that result in very similar levels of MRO as determined by XRD, the two materials remain very different in their bonded H content and apparently in their H distributions as detected by NMR [1,16]. There are no HRTEM studies yet that have identified nanoscale ordered regions in the HWCVD material, in contrast to such observations for the PECVD films. Such material containing nanometer-sized ordered features has recently shown evidence of faster crystallization under annealing [10]. This may be a sensitive method for the detection of such features. It would be interesting to probe via cross-sectional TEM the depth distribution and morphology of the microcrystallites that develop in the high-hydrogen-dilution PECVD films as the thickness is increased. Such recent studies of HWCVD films show cone-shaped crystals that appear to extend from near the substrate-film interface to the surface for a film 74 nm in thickness. It would be surprising if this occurs in the samples studied here which can show no evidence of microcrystallinity until thicknesses in excess of 1000 nm are reached.

An important implication of the observed thickness- and substrate-dependent changes in MRO, microcrystalline fraction, and defect density of the material prepared near the a-Si:H/mc-Si:H boundary is that films made for various property measurements requiring differing thicknesses or substrates will likely give conflicting results.

Perhaps modeling studies along the lines recently described [24,25,28] could examine which type of changes in MRO can induce the width changes in the FSP documented here.

3.1.2 SAXS from NREL HWCVD a-Si:H

A set of HWCVD samples was prepared by NREL to examine the nanostructure of a-Si:H material grown in the "T" system with deposition rates of 1 to 2 nm/s. The deposition conditions for the four samples are shown in Table 1. Figure 6 compares the SAXS from the four samples where one can see much stronger intensities from the two samples that used the lower substrate temperature (T_s = 280°C). This is consistent with prior results that demonstrated higher temperatures lead to much less heterogeneity in HWCVD material [32]. Table 2 summarizes the quantitative SAXS results and shows the dramatic increase in nanovoid volume fractions in the lower T_s films. Also, the lower void fraction for T905 compared to T841 (both at T_s = 360°C)

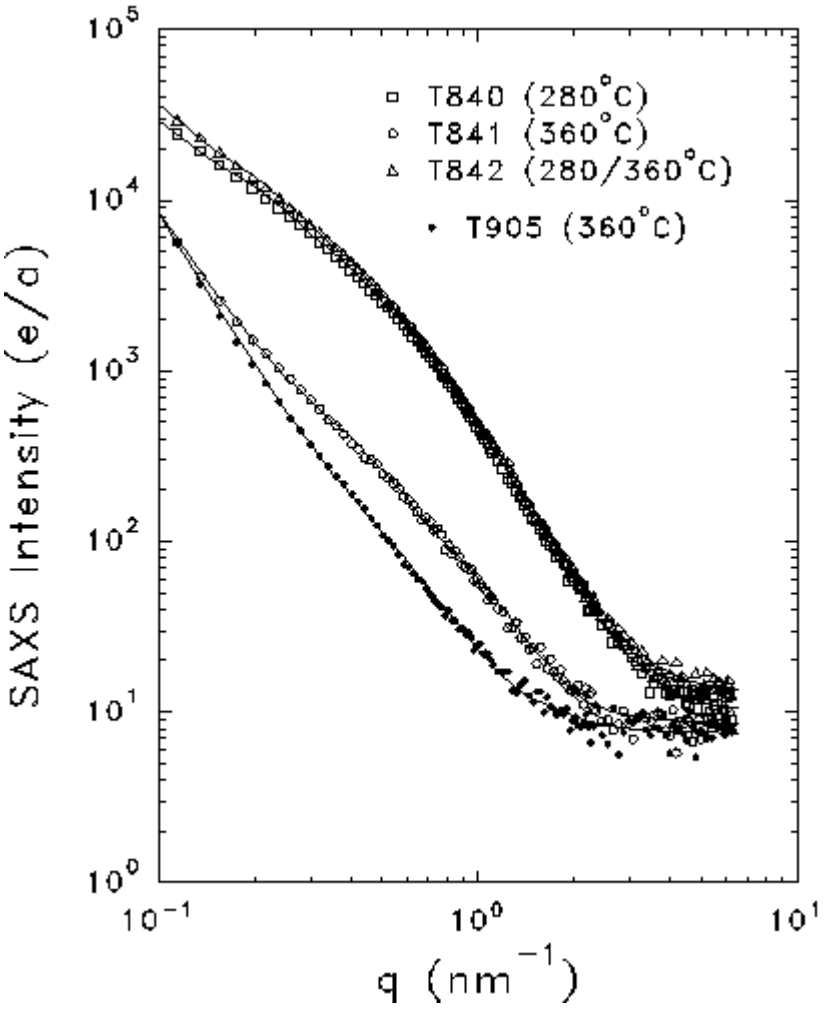

FIG. 6. SAXS from HWCVD a-Si:H films for various substrate temperatures.

indicates a possible effect due to H plasma treatment. The lower values of diffuse scattering intensity (I_D) for these higher T_s films are consistent with a lower H content.

Table 1. Deposition conditions for NREL HWCVD samples

Sample	T_s (°C)	Thickness (μm)	Dep. Rate (nm/s)	Conditions
T840	280	1.7	1.4	20 min dep; cooled in H_2; 10 min H plasma
T841	360	1.9	1.5	20 min dep; cooled in H_2; 10 min H plasma
T842	280/360	1.2	1.0	10 min dep @ 280°C then 10 min dep @ 360°C; cooled in H_2; 10 min H plasma
T905	360	3.7	1.5	40 min dep; cooled in Ar in load lock

Table 2. SAXS results from NREL HWCVD films

Sample	T_s (°C)	Q_N (10^{23}eu/cm^3)	f (vol.%)	<D> (nm)	A (eu/nm^3)	I_D (eu)
T840	280	33.5	2.	8.2	16	10
T841	360	2.4	0.14	6.2	8	8.5
T842	280/360	36.5	2.1	8.2	22	13
T905	360	0.5	0.03	5.7	8	7.5

Q_N = integrated SAXS intensity due to nano-scale features;
f = nanovoid volume fraction assuming all of Q_N is due to voids;
<D> = average diameter of nanoscale features (spheres assumed in fits);
A = Porod constant in $I_L = A/q^3$ term used to fit data at lowest q;
I_D = diffuse scattering intensity;
eu = electron units = e/a = electrons/atom.

3.1.3 SAXS from MVS PECVD and HWCVD a-Si:H

Figure 7 compares SAXS from the two MVSystems (MVS) films prepared by PECVD and HWCVD and one can see dramatic differences. The solid lines are fits to the data based on the sum of contributions $I_L + I_N + I_D$, as described in my review paper [32] due to larger scale structure, nanoscale structure, and atomic-scale composition fluctuations. Qualitatively, the HWCVD sample is dominated by larger-scale structure as seen by the continuously rising signal as q becomes smaller, while the PECVD sample has no detectable larger-scale structure since the signal seems to saturate at smaller q. The background diffuse signal (I_D) is larger for the PECVD and this is attributed to a much higher bonded H content is this sample. In fact the very low I_D for the

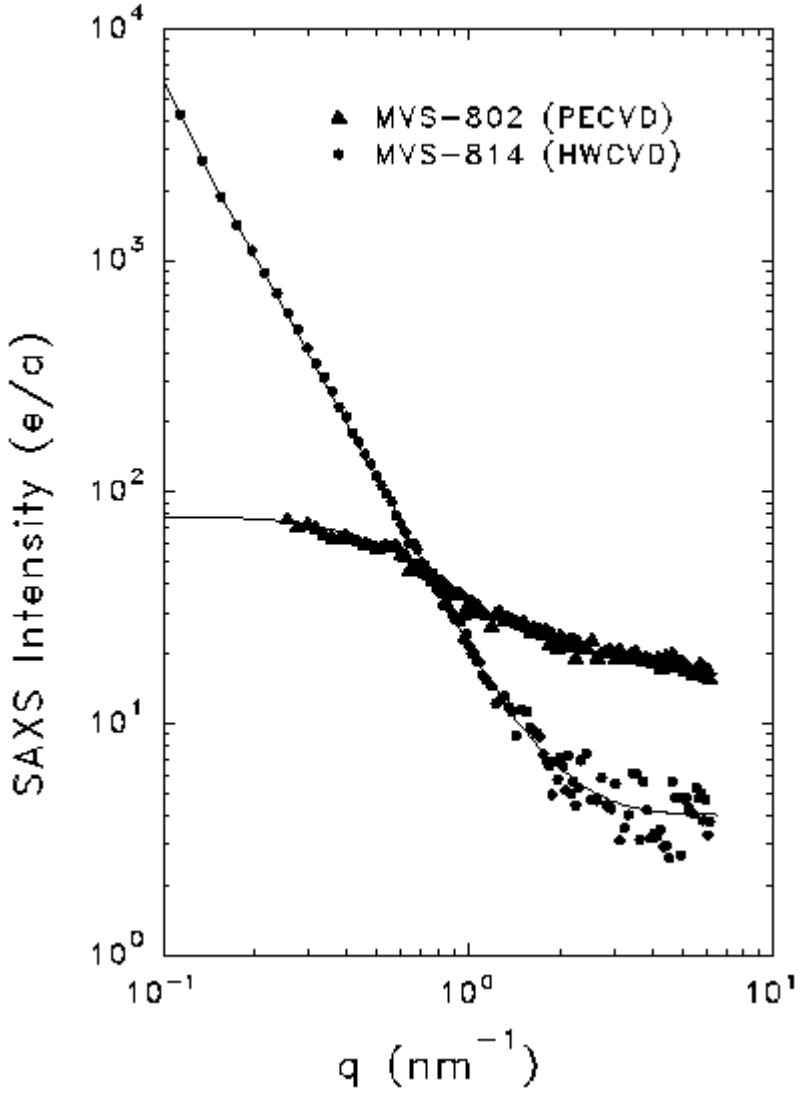

FIG. 7. SAXS from MVSystems films made by PECVD and HWCVD.

HWCVD sample indicates quite a low H content and therefore a high substrate temperature. This is consistent with the fact that we detected microcrystallinity in the HWCVD film via X-ray diffraction measurements. This was likely induced by interdiffusion-induced crystallization caused by the Al substrate. We have established that substrate temperatures near or above 450°C can cause this effect. Table 3 presents a summary of the quantitative results from fitting the SAXS data. The volume fractions of nanovoids are quite small but significantly larger than our detection limit of 0.01%.

Table 3. SAXS results from MVS samples

Sample	Dep. Method	t_p (μm)	t_x (μm)	Q_N (10^{23}eu/cm^3)	f (vol.%)	<D> (nm)	A (eu/nm^3)	I_D (eu)
MVS802	PECVD	1.9	3.61	2.4	0.14	1.2	0	15
MVS814	HWCVD	2.1	3.55	1.1	0.06	8.6	5.5	4

t_p = thickness provided by MVS;
t_x = thickness determined by x-ray absorption;
Other symbols same as defined in Table 2.

3.1.4 Effect of Deposition Rate on Nanostructure via RF- and VHF-PECVD of a-Si:H

The effect of deposition rate on the nanostructure of PECVD a-Si:H has been examined in collaboration with ECD. Three deposition rates were used for both the standard RF method (13.56 MHz) and the VHF method (70 MHz). Figure 8 shows the systematic increase in SAXS as the deposition rate is increased for RF material. Figure 9 compares quantitative SAXS results for the two deposition methods and shows systematic differences. The VHF material retains reduced nanostructure (Q_N), less large-scale structure (Porod slope = A), and less bonded hydrogen (smaller I_D) as the deposition rate increases. Further work is in progress to be sure that other deposition conditions that were changed to increase the deposition rate are not responsible for the differences in the SAXS observations.

3.2 LOW-GAP MATERIALS

3.2.1 Thickness dependence of nanostructure in a-SiGe:H

Three films were prepared by PECVD at ECD for study by SAXS. Sample L3165 was a standard device-quality a-Si:H film of total thickness 0.9 μm, sample L3166 was a standard device-

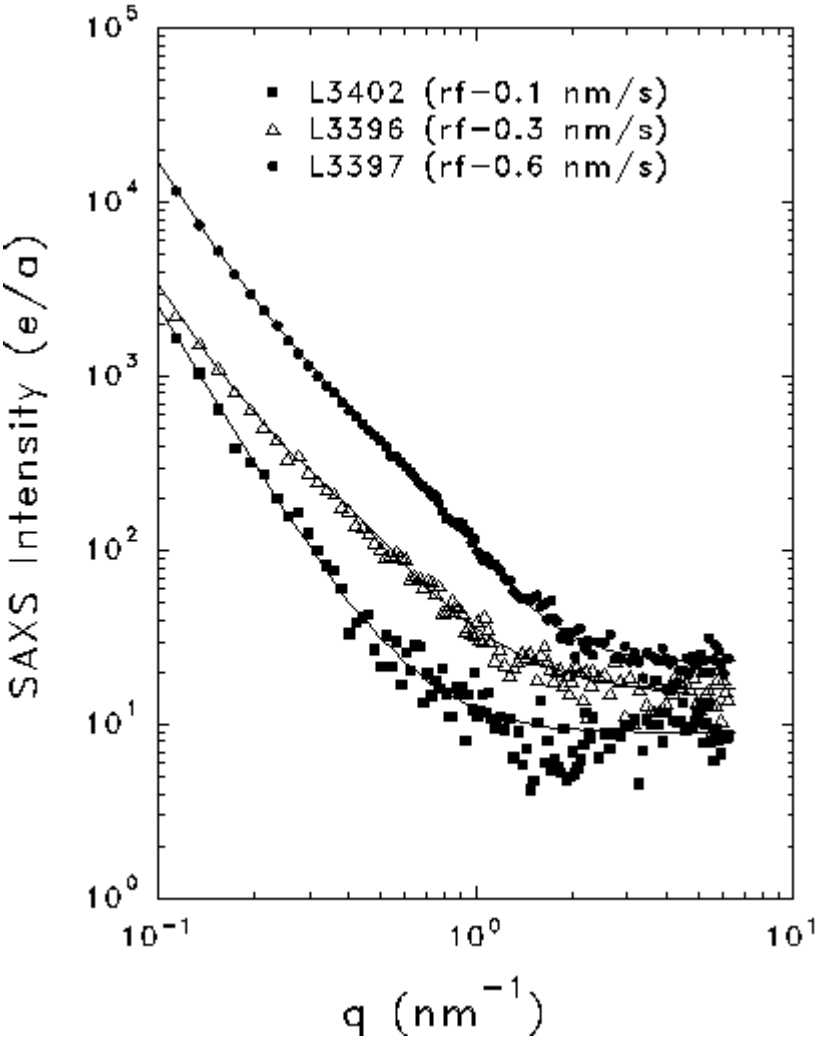

FIG. 8. SAXS versus deposition rate of RF-PECVD a-Si:H.

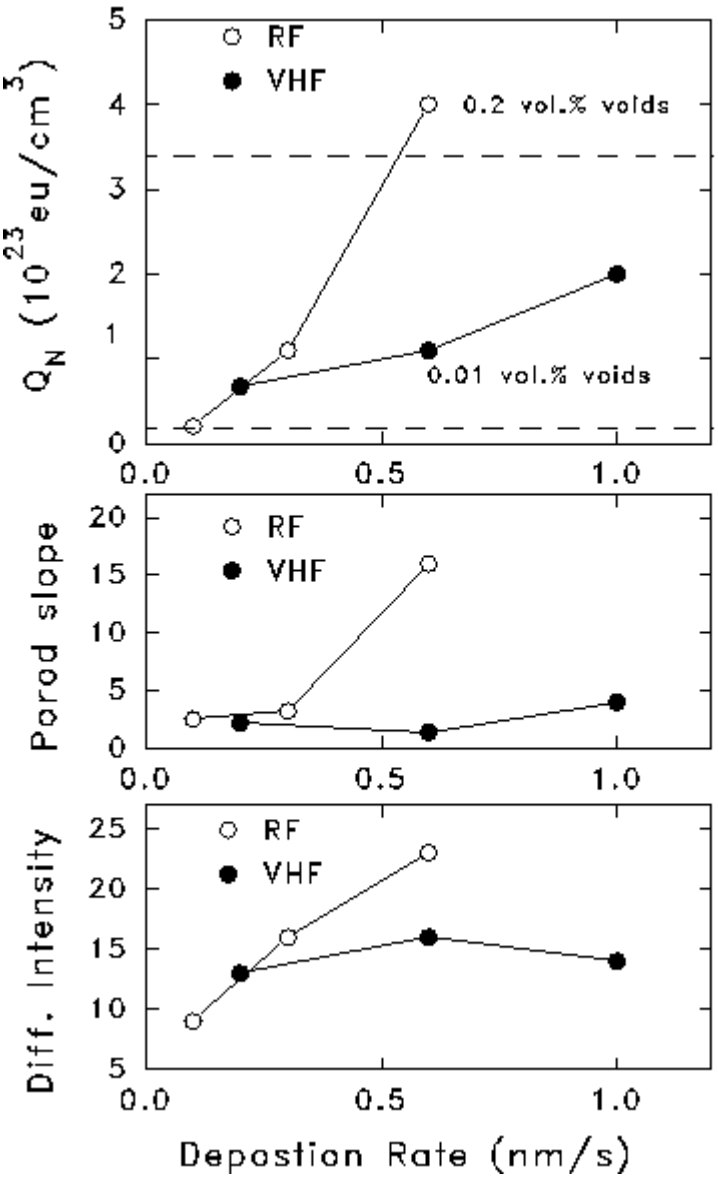

FIG. 9. Comparison of SAXS results for RF and VHF a-Si:H versus deposition rate.

quality a-SiGe:H film of total thickness 1.3 μm, and sample L3167 was a multilayer film consisting of 5 alternating layers of a-Si:H (0.05 μm each) and a-SiGe:H (0.20 μm each), prepared under the same conditions used for the individual films L3165 and L3166, respectively. A comparison of the nanostructure would address the question of whether there is a change in the a-SiGe:H as the film is grown thicker than 0.2 μm. Figure 10 shows plots of the SAXS results from the 3 samples and the associated size distributions obtained assuming spherical scattering objects. Since the SAXS intensities are presented in absolute units, thickness effects have been removed and a direct comparison is possible. Qualitatively, there appears to be only a small difference between the a-SiGe:H sample and the a-SiGe:H/a-Si:H multilayer. The slight difference at lower q may be due to the a-Si:H contribution. Indeed, the size distribution of the multilayer seems to be a composite of the two individual layers. Quantitatively, all the results are as follows:

Table 4. SAXS results for ECD a-$Si_{1-x}Ge_x$:H films. Symbols same as in Table 2.

Sample	Thickness (μm)	x (via EPMA)	Q_N (10^{24}eu/cm^3)	I_D (eu)	A (eu/nm^3)	<D> (nm)
L3165	0.9	--	0.05	10	0.7	2.9
L3166	1.3	0.36	1.80	64	2.4	1.55
L3167	1.4	0.37	1.66	73	4.3	1.83

It is surprising that the EPMA result for the multilayer (L3167) is higher than for the pure a-SiGe:H (L3166). An expected value would be (based on the relative thicknesses) an average of 80% x 0.36 + 20% x 0.00 = 0.29. However, the larger I_D for L3167 is consistent with the larger average x via EPMA. The thicknesses shown in Table 4 are from the x-ray absorption and are slightly different than expected from the designed preparation conditions for the a-SiGe. The smaller Q_N for the L3167 is not obvious in the figure but the slightly larger sizes shift the data to smaller q and therefore the integrated SAXS is smaller. (The Q_N does not include the A/q^3 term). It is interesting that these values for Q_N are somewhat smaller than those summarized in a previous comparison of several samples and techniques [47]. Tilting experiments will be done eventually to look for any oriented structural difference. The conclusion from this study is that there is no obvious change in the nanostructure of device-quality, PECVD a-SiGe:H when the thickness is increased from 0.2 to 1.3 μm.

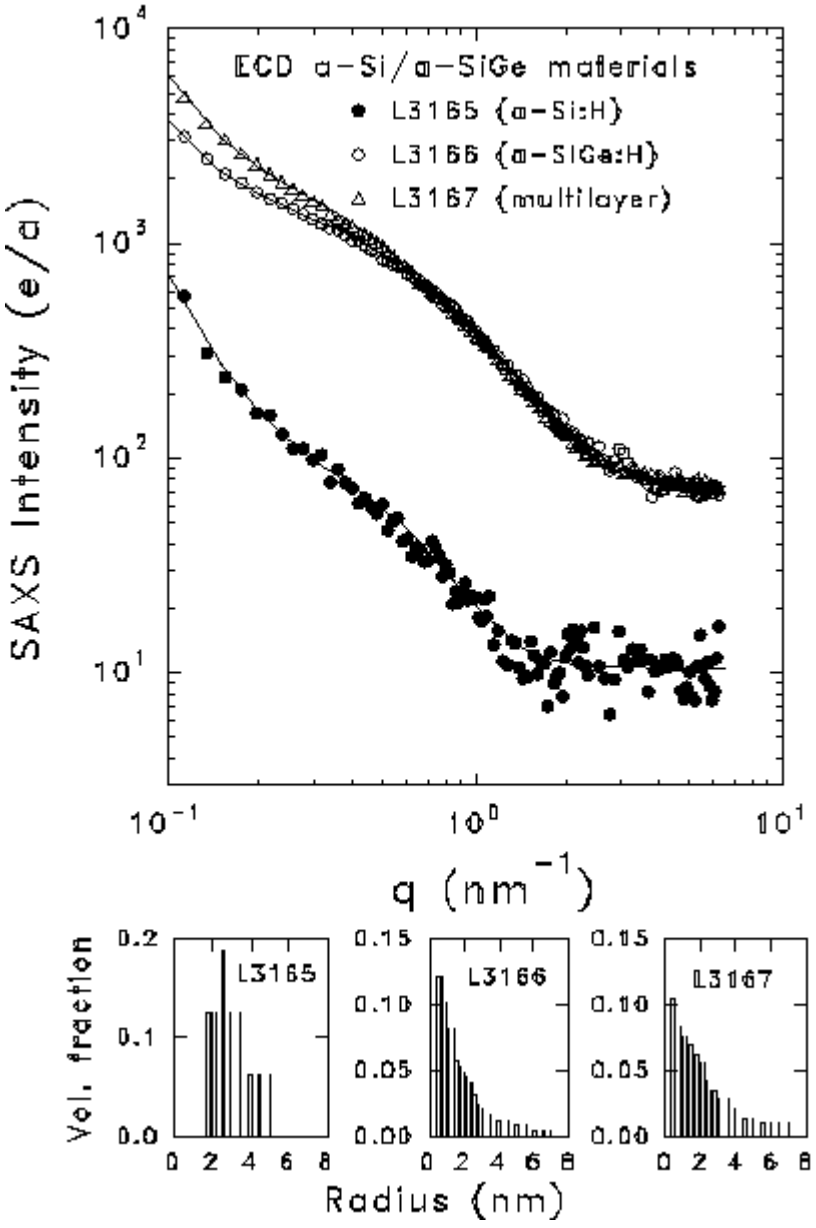

FIG. 10. SAXS data from ECD films and corresponding size distributions used to generate the solid lines through the SAXS data.

3.3 SANS EXPERIMENTS

3.3.1 Proposal for Beam Time

Our proposal for SANS beam time at the NIST Center for Neutron Research was successful and three days have been awarded beginning August 9, 1999. Only 32 of the 72 proposals submitted were awarded beam time. (Copy of proposal available upon request)

3.3.2 Sample Preparation

The special samples required for these studies are being designed in collaboration with NREL and USSC and will be prepared during June and July, 1999. A summary of the requested samples is given in Table 5. The deuterated gases (SiD_4, GeD_4, and D_2) as well as ultra-smooth c-Si wafers (≤ 0.5 nm roughness) to be used as substrates have all been ordered. AFM measurements will be made to test the roughness. NREL will prepare the HWCVD samples and USSC will prepare the PECVD samples. A critical issue in the preparation of these samples will be the adhesion of the films to the c-Si. Some of the a-Si:H films will be light soaked as long as possible before going to NIST.

Table 5. Samples requested for SANS experiments.

Sample	Film grower	Gases	Thickness (μm)	Growth method
a-Si:H	USSC	SiH_4, H_2	20	PECVD - high hydrogen dilution
a-Si:D	USSC	SiD_4, D_2	20	PECVD - high deuterium dilution
a-Si:H	USSC	SiH_4	20	PECVD - no hydrogen dilution
a-Si:D	USSC	SiD_4	20	PECVD - no deuterium dilution
a-SiGe:H	USSC	SiH_4,GeH_4,H_2	10	PECVD - high hydrogen dilution
a-SiGe:D	USSC	SiD_4,GeD_4,D_2	10	PECVD - high deuterium dilution
a-Si:H	NREL	SiH_4	20	HWCVD - high substrate temp.
a-Si:D	NREL	SiD_4	20	HWCVD - high substrate temp
a-Si:H	NREL	SiH_4	20	HWCVD - low substrate temp.
a-Si:D	NREL	SiD_4	20	HWCVD - low substrate temp.
a-SiGe:H	NREL	SiH_4, GeH_4	10	HWCVD - high substrate temp.
a-SiGe:D	NREL	SiD_4, GeD_4	10	HWCVD - high substrate temp.
a-SiC:H	NREL	SiH_4,CH_4	10	PECVD
μc-Si:H	NREL	SiH_4, H_2	10	HWCVD or PECVD

4. REFERENCES

1. K-C. Hsu and H-L. Hwang, Appl. Phys. Lett. **61**, 2075 (1992).
2. X. Xu, J. Yang, and S. Guha, J. Non-Cryst. Solids **198-200**, 60 (1996).
3. U. Kroll, J. Meier, A. Shah, S. Mikhailov, and J. Weber, J. Appl. Phys. **80**, 4971 (1996).
4. D.V. Tsu, B.S. Chao, S.R. Ovshinsky, S. Guha, and J. Yang, Appl. Phys. Lett. **71**, 1317 (1997).
5. P. Roca i Cabarrocas, S. Hamma, S.N. Sharma, G. Viera, E. Bertran, and J. Costa, J. Non-Cryst. Solids **227-230**, 871 (1998).
6. J. Koh, H Fujiwara, R.W. Collins, Y. Lee, and C.R. Wronski, J. Non-Cryst. Solids **227-230**, 73 (1998).
7. U. Kroll, J. Meier, P. Torres, J. Pohl, and A. Shah, J. Non-Cryst. Solids **227-230**, 68 (1998).
8. S. Sheng, X. Liao, G. Kong, and H. Han, Appl. Phys. Lett. **73**, 336 (1998).
9. J.H. Koh, Y.H. Lee, H. Fujiwara, C.R. Wronski, and R.W. Collins, Appl. Phys. Lett. **73**, 1526 (1998).
10. E. Bertran, S.N. Sharma, G. Viera, J. Costa, P. St'ahel, and P. Roca i Cabarrocas, J. Mater. Res. **13**, 2476 (1998).
11. T. Kamei, P. Stradins, and A. Matsuda, Appl. Phys. Lett. 74, 1707 (1999).
12. S. Guha, J. Yang, D.L. Williamson, Y. Lubianiker, J.D. Cohen, and A.H. Mahan, Appl. Phys. Lett. **74**, 1860 (1999).
13. A.H. Mahan, J. Carapella, B.P. Nelson, and R.S. Crandall, J. Appl. Phys. **69**, 6728 (1991).
14. P. Papadopulos, A. Scholz, S. Bauer, B. Schröder, and H. Oechsner, J. Non-Cryst. Solids **164-166**, 87 (1993).
15. M. Heintze, R. Zedlitz, H.N. Wanka, and M.B. Schubert, J. Appl. Phys. **79**, 2699 (1996).
16. Y. Wu, J.T. Stephen, D.X. Han, J.M. Rutland, R.S. Crandall, and A.H. Mahan, Phys. Rev. Lett. **77**, 2049 (1996).
17. Xiao Liu, B.E. White, Jr., R.O. Pohl, E. Iwanizcko, K.M. Jones, A.H. Mahan, B.N. Nelson, R.S. Crandall, and S. Veprek, Phys. Rev. Lett. **78**, 4418 (1997).
18. A.H. Mahan, D.L. Williamson, and T.E. Furtak, Mat. Res. Soc. Symp. Proc. **467**, 657 (1998).
19. Z. Remes, M. Vanecek, P. Torres, U. Kroll, A.H. Mahan, and R.S. Crandall, J. Non-Cryst. Solids **227-230**, 876 (1998).
20. S. Bauer, B. Schröder, and H. Oechsner, J. Non-Cryst. Solids **227-230**, 34 (1998).

21. A.M. Brockhoff, E.H.C. Ullersma, H. Meiling, F.H.P.M. Habraken, and W.F. van der Weg, Appl. Phys. Lett. **73**, 3244 (1998).
22. S.C. Moss and D.L. Price, in *Physics of Disordered Materials*, edited by D. Adler, H. Fritzsche, and S.R. Ovshinsky (Plenum, New York, 1985) p.77.
23. S.R. Elliott, Nature **354**, 445 (1991); J. Phys.:Condens. Matter **4**, 7661 (1992).
24. L. Cervinka, J. Non-Cryst. Solids **232-234**, 1 (1998).
25. K. Tanaka, Jpn. J. Appl. Phys. **37**, 1747 (1998).
26. J. Bletry, Phil. Mag. B **62**, 469 (1990).
27. J. Dixmier, J. Phys. I France **2**, 1011 (1992).
28. A. Uhlherr and S.R. Elliott, Phil. Mag. B **71**, 611 (1995).
29. M. Essamet, B. Hepp, N. Proust, and J. Dixmier, J. Non-Cryst. Solids **97&98**, 191 (1987).
30. B.E. Warren, *X-ray Diffraction* (Addison-Wesley, Reading MA, 1969).
31. A.P. Sokolov, A. Kisliuk, M. Soltwisch, and D. Quitmann, Phys. Rev. Lett. **69**, 1540 (1992).
32. D.L. Williamson, Mat. Res. Soc. Symp. Proc. **377**, 251 (1995).
33. M.M.J. Treacy and J.M. Gibson, Acta Cryst. **A52**, 212 (1996).
34. J.M. Gibson, M.M.J. Treacy, P.M. Voyles, H-C. Jin, and J.R. Abelson, Appl. Phys. Lett. **73**, 3093 (1998).
35. J. Yang, A. Banerjee, and S. Guha, Appl. Phys. Lett. **70**, 2975 (1997).
36. A.H. Mahan, R.C. Reedy Jr., E. Iwaniczko, Q. Wang, B.P. Nelson, Y. Xu, A.C. Gallagher, H.M. Branz, R.S. Crandall, J. Yang, and S. Guha, Mat. Res. Soc. Symp. Proc. **507**, 119 (1998).
37. P. Roca i Cabarrocas, N. Layadi, T. Heitz, B. Drevillon, and I. Solomon, Appl. Phys. Lett. **66**, 3609 (1995).
38. H. Shirai, Jpn. J. Appl. Phys. **34**, 450 (1995).
39. R. Ossikovski and B. Drevillon, Phys. Rev. B **54**, 10530 (1996).
40. M. Tozlov, F. Finger, R. Carius, and P. Hapke, J. Appl. Phys. **81**, 7376 (1997).
41. L.L. Smith, E. Srinivasan, and G.N. Parsons, J.Appl. Phys. **82**, 6041 (1997).
42. A.H. Mahan, M. Vanacek, A. Poruba, V. Vorlicek, R.S. Crandall, and D.L. Williamson, Mat. Res. Soc. Symp. Proc. **507**, 825 (1998).
43. A.H. Mahan and M. Vanacek, AIP Conf. Proc. **234**, 211 (1991).
44. S. Guha, Current Opinion in Solid State and Materials Science **2**, 425 (1997).

45. M Shima, M. Isomura, E. Maruyama, S. Okamoto, H. Haku, K. Wakisaka, S. Kiyama, and S. Tsuda, Jpn. J. Appl. Phys. **37**, 6322 (1998).
46. R. Platz, S. Wagner, C. Hof, A. Shah, S. Wieder, and B. Rech, J. Appl. Phys. **84**, 3949 (1998).
47. D.L. Williamson, Y. Xu, and B.P. Nelson, in NCPV Photovoltaics Program Review, Proceedings of the 15th Conference, AIP Conf. Proc. **462**, edited by M. Al-Jassim, J.P. Thornton, and J.M. Gee (AIP, Woodbury, NY, 1999) p. 272.

REPORT DOCUMENTATION PAGE

Form Approved
OMB NO. 0704-0188

1. AGENCY USE ONLY (Leave blank)	2. REPORT DATE	3. REPORT TYPE AND DATES COVERED
	December 1999	Annual Technical Progress Report, 22 May 1998–21 May 1999

4. TITLE AND SUBTITLE
Nanostructure of a-Si:H and Related Alloys by Small-Angle Scattering of Neutrons and X-Rays

5. FUNDING NUMBERS
C: XAK-8-17619-31
TA: PV005001

6. AUTHOR(S)
D.L. Williamson

7. PERFORMING ORGANIZATION NAME(S) AND ADDRESS(ES)
Department of Physics
Colorado School of Mines
Golden, CO 80401

8. PERFORMING ORGANIZATION REPORT NUMBER

9. SPONSORING/MONITORING AGENCY NAME(S) AND ADDRESS(ES)
National Renewable Energy Laboratory
1617 Cole Blvd.
Golden, CO 80401-3393

10. SPONSORING/MONITORING AGENCY REPORT NUMBER
SR-520-27664

11. SUPPLEMENTARY NOTES
NREL Technical Monitor: B. von Roedern

12a. DISTRIBUTION/AVAILABILITY STATEMENT
National Technical Information Service
U.S. Department of Commerce
5285 Port Royal Road
Springfield, VA 22161

12b. DISTRIBUTION CODE

13. ABSTRACT (Maximum 200 words)
This report describes work being performed to provide details of the microstructure in high-quality hydrogenated amorphous silicon and related alloys on the nanometer scale. The materials under study are being prepared by state-of-the-art deposition methods, as well as by new and emerging deposition techniques. The purpose is to establish the role of nanostructural features in controlling opto-electronic and photovoltaic properties. The approach centers around the use of the uncommon technique of small-angle scattering of both X-rays (SAXS) and neutrons (SANS). SAXS has already been established as highly sensitive to microvoids and columnar-like microstructure. A major goal of this research is to establish the sensitivity of SANS to the hydrogen nanostructure. Conventional X-ray diffraction techniques are being used to examine medium-range order and microcrystallinity, particularly near the boundary between amorphous and microcrystalline material.

14. SUBJECT TERMS
photovoltaics ; nanostructures ; amorphous silicon ; small-angle scattering ; microcrystalline material

15. NUMBER OF PAGES

16. PRICE CODE

17. SECURITY CLASSIFICATION OF REPORT	18. SECURITY CLASSIFICATION OF THIS PAGE	19. SECURITY CLASSIFICATION OF ABSTRACT	20. LIMITATION OF ABSTRACT
Unclassified	Unclassified	Unclassified	UL